Magnetic Resonance Imaging 62 (2019) 159–166

Contents lists available at ScienceDirect

Magnetic Resonance Imaging

journal homepage: www.elsevier.com/locate/mri

Original contribution

Coronary vessel wall visualization via three-dimensional turbo spin-echo black blood imaging in Kawasaki disease

Koji Matsumoto[a,b,*], Hajime Yokota[c], Hiroki Mukai[c], Ryota Ebata[d], Naoki Saito[d], Kenji Shimokawa[a], Takafumi Yoda[a], Yoshitada Masuda[a], Takashi Uno[c], Tosiaki Miyati[b]

[a] Department of Radiology, Chiba University Hospital, 1-8-1 Inohana, Chuo-ku, Chiba, Chiba 260-8677, Japan
[b] Division of Health Sciences, Graduate School of Medical Sciences, Kanazawa University, 5-11-80 Kodatsuno, Kanazawa, Ishikawa 920-0942, Japan
[c] Diagnostic Radiology and Radiation Oncology, Graduate School of Medicine, Chiba University, 1-8-1 Inohana, Chuo-ku, Chiba, Chiba 260-8670, Japan
[d] Department of Pediatrics, Graduate School of Medicine, Chiba University, 1-8-1, Inohana, Chuo-ku, Chiba, Chiba 260-8670, Japan

ARTICLE INFO

Keywords:
Kawasaki disease
Black blood imaging
Vessel wall imaging
Coronary artery
Turbo spin-echo

ABSTRACT

Purpose: To evaluate the feasibility of coronary vessel wall visualization using three-dimensional turbo spin-echo black blood imaging (3D-TSE) in children with Kawasaki disease.

Materials and methods: Nine patients (6 girls and 3 boys; mean age ± standard deviation, 5.6 ± 3.3 years; range, 1.4–10.3 years) were included. Coronary magnetic resonance angiography (MRA) with an axial slice orientation and 3D-TSE with axial and sagittal slice orientations (3D-TSE-axi and 3D-TSE-sag) were acquired for the whole heart. Coronary vessel walls were evaluated separately in aneurysm and normal-proximal regions. The internal diameter and wall thickness of the reformatted cross-sectional images were measured in both the regions. Reproducibility between MRA and 3D-TSE was evaluated via interclass correlation coefficients (ICCs) and Bland-Altman plots.

Results: In total, 164 points (aneurysmal regions, 73; normal-proximal regions, 64; normal-distal regions, 27) were evaluated. The ICC for 3D-TSE-axi was higher than that for 3D-TSE-sag (aneurysmal regions, ICC = 0.88 and 0.81; normal-proximal regions, ICC = 0.90 and 0.32, respectively). Bland-Altman plots of the internal diameter via MRA and 3D-TSE-axi showed a wide 95% limit of agreement (−0.13 to 2.89 mm) and significant fixed and proportional biases ($P < 0.001$ and $P = 0.002$) in the aneurysmal regions. However, the 95% limit of agreement was narrow (−0.14 to 0.57 mm) in the normal-proximal regions. If 1 mm was set as the cut-off for a thickened wall, wall thickness via 3D-TSE-axi was found to be abnormal across many points (84.0% of aneurysmal regions; 18.4% of normal-proximal regions).

Conclusions: 3D-TSE imaging of the normal-proximal regions of the coronary vessel in individuals with Kawasaki disease was found to be feasible. However, in aneurysmal regions, larger aneurysmal diameters led to an increased bias between MRA and 3D-TSE.

1. Introduction

Kawasaki disease (KD) is an acute vasculitis of unknown etiology that usually occurs in children below five years of age and often involves formation of coronary artery aneurysms [1]. Coronary artery aneurysms can rupture, thrombose, and lead to the development of stenotic lesions. Some of these children need anti-thrombotic therapy, percutaneous coronary interventions [2] or/and coronary bypass operations [3]. Thus, serial evaluation of the size and location of aneurysms is essential to decide therapeutic strategy and follow the patients [4]. Coronary magnetic resonance angiography (MRA) using three-dimensional (3D) balanced steady-state free precession imaging, a minimally invasive procedure, is used for the evaluation of coronary arterial lesions in KD [5]. MRA is equivalent to X-ray coronary angiography (XCA) for the identification of coronary artery aneurysms in patients with KD [6–9]. However, MRA does not allow for sufficient

Abbreviations: 3D-TSE, three-dimensional turbo spin-echo black blood imaging; KD, Kawasaki disease; MRA, magnetic resonance angiography; ICC, interclass correlation coefficient; XCA, X-ray coronary angiography; TTE, transthoracic echocardiography; RCA, right coronary artery; LCA, left coronary artery; SPIR, spectral inversion recovery; AHA, American Heart Association; IR, inversion-recovery; DIR, dual inversion-recovery; GRE, gradient-echo

* Corresponding author at: Department of Radiology, Chiba University Hospital, 1-8-1 Inohana, Chuo-ku, Chiba-shi, Chiba 260-0856, Japan.
E-mail addresses: matumoto@chiba-u.jp (K. Matsumoto), hjmykt@chiba-u.jp (H. Yokota), eba-ryo@chiba-u.jp (R. Ebata), t-yoda@chiba-u.jp (T. Yoda), masuda.yoshitada@hospital.chiba-u.jp (Y. Masuda), unotakas@faculty.chiba-u.jp (T. Uno), ramiyati@mhs.mp.kanazawa-u.ac.jp (T. Miyati).

https://doi.org/10.1016/j.mri.2019.07.001
Received 2 February 2019; Received in revised form 22 May 2019; Accepted 1 July 2019

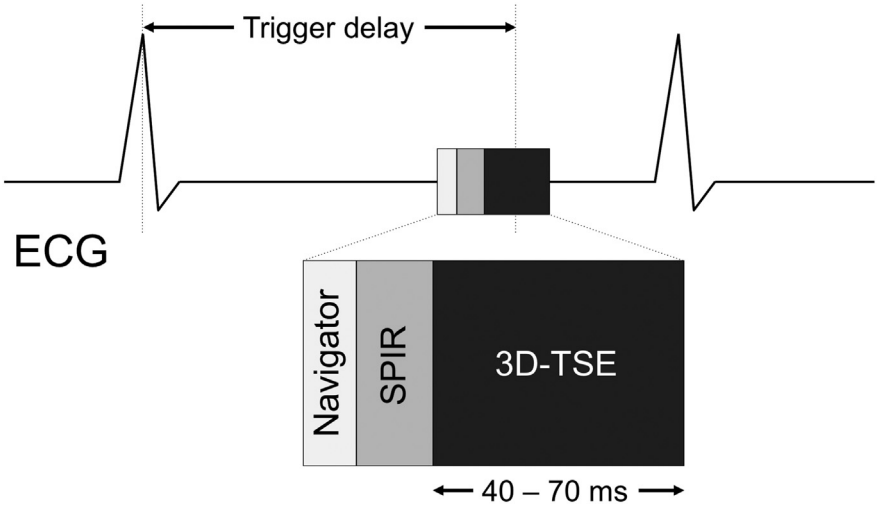

Fig. 1. Imaging diagram depicting the procedure for free-breathing navigator-gated three-dimensional turbo spin-echo (3D-TSE) black blood imaging. To suppress epicardial fat signals, a spectral inversion recovery (SPIR) pulse was applied. Imaging was performed during mid-diastole or systole, which is a quiescent period in the cardiac cycle.

detection of thrombi and intimal proliferation. Therefore, coronary wall imaging is preferred [9–16].

Two-dimensional (2D) imaging was used for pediatric coronary vessel wall imaging in previous reports [8,9]. 2D imaging has a high in-plane resolution but suffers from a relatively limited coverage of the pediatric coronary artery tree. Hence, a 3D approach facilitating more extensive coverage is desirable [14]. 3D imaging also allows for easy visualization of accurate cross sections with less partial volume effect after post-processing. 3D turbo spin-echo (TSE) using a variable flip-angle refocusing pulse sequence (e.g., VISTA, SPACE, CUBE) has a sequence-endogenous blood signal void and is thus a promising technique for black-blood imaging [17–19]. Given this advantage, 3D-TSE has been widely used for imaging of the carotid and intracranial arterial vessel walls [20–22]. Despite this, coronary vessel wall imaging remains vulnerable to heartbeat- and respiration-derived motion artifacts. These artifacts can render the pulse sequence unusable. Furthermore, 3D-TSE has strong directivity in the acquisition section and flow direction; however, the most appropriate direction for imaging pediatric coronary arteries remains unclear.

Therefore, in the present study, we used cardiac-triggered and real-time navigator echo methods [23] in 3D-TSE to reduce the effects of heartbeat- and respiration-induced movement artifacts. We then examined the feasibility of coronary vessel wall imaging in children with KD by changing the slice orientation of 3D-TSE and comparing resultant images both visually and quantitatively.

2. Materials and methods

2.1. Subjects

The patients' families provided informed consent, and this study was approved by the local ethics committee. We enrolled nine patients (6 girls and 3 boys; mean age ± standard deviation [SD]: 5.6 ± 3.3 years; range, 1.4–10.3 years) who underwent cardiac magnetic resonance imaging (MRI) between March 2014 and December 2015. These patients were undergoing follow-up care for a transient dilated lesion of the coronary artery during the acute phase of KD or coronary arterial lesions such as aneurysms and stenosis resulting from KD.

Transthoracic echocardiography (TTE) [24] and XCA revealed aneurysms at 21 sites in the nine patients (right coronary artery [RCA]: 8; left coronary artery [LCA]: 13). The detected range of heart rates during MRI was 72 to 108 beats per minute (BPM) (mean ± SD: 91.3 ± 10.9 BPM). To achieve mild patient sedation during the MRI examination, all patients were given sodium trichloroethylene phosphate syrup (0.7 to 0.8 mL/kg). If the syrup was ineffective, patients were administered thiopental sodium (2 to 3 mg/kg) or midazolam (0.2 mg/kg) via IV infusion to achieve unconscious sedation for the duration of imaging. Patients' coronary arteries were then routinely imaged via TTE and XCA (five and four patients, respectively). The interval between cardiac MRI and transthoracic echocardiography was 0 to 28 days (mean ± SD, 14.6 ± 13.6 days) whereas that between cardiac MRI and XCA was consistently three days. No thromboses were identified via transthoracic echocardiography or XCA. No adverse clinical events occurred during the period between cardiac MRI and transthoracic echocardiography or XCA.

2.2. Data acquisition

All MR imaging studies were performed with 1.5-T MR imaging units (Intera Achieva Nova-Dual release 3.2, Philips Medical Systems, Best, Netherland) with a two-element flex-medium coil or a five-element synergy cardiac coil. First, a high-resolution 2D cine scan with an axial slice orientation was used to identify the precise period of minimal cardiac motion for each patient. Subsequently, MRA with an axial slice orientation and 3D-TSE with both axial and sagittal slice orientations (3D-TSE-axi and 3D-TSE-sag) were used to image the whole heart.

MRA images were obtained using the following parameters: a free-breathing navigator-gated and cardiac-triggered bright blood 3D balanced steady-state free precession (3D balanced turbo field echo) with a repetition time (TR) of 4.2 ms; echo time (TE) of 2.1 ms; flip angle of 90°; resolution of 1.2 × 1.2 × 1.1 to 1.6 mm (reconstruction, 0.6 × 0.6 × 0.55 to 0.8 mm); slice number of 90 to 110; and spectral inversion recovery (SPIR). The total scan time was 2 min 59 s with 100% navigator efficiency (calculated for a heart rate of 80 BPM).

3D-TSE images were obtained with the following parameters: a free-breathing navigator-gated and cardiac-triggered 3D turbo spin-echo with a TR equivalent to the duration of one heartbeat (522 to 800 ms); TE of 29 to 44 ms; flip angle of 90°; refocusing flip angle of 50°; turbo factor of 9 to 15; resolution of 1.2 × 1.2 × 1.1 to 1.6 mm (reconstruction, 0.6 × 0.6 × 0.55 to 0.8 mm); slice number of 90 to 110; SPIR; and flow-sensitizing to suppress the blood signal [25]. The total scan time was 4 min 50 s with 100% navigator efficiency (calculated for a heart rate of 80 BPM) (Fig. 1). All sequences were equipped with a right hemidiaphragmatic prospective real-time navigator for respiratory motion artifact suppression in freely breathing patients [23]. Data were accepted if the lung-liver interface was within the end-expiratory gating window (2 to 4 mm) or were rejected and reacquired during the subsequent inter-beat interval. A 50-degree refocusing flip angle was used to increase saturation. Flowing spin in fast spin-echo imaging arises from two primary mechanisms: intravoxel dephasing from isochromats with different velocities, and mixing among pathways involving

different combinations of spin echoes and stimulated echoes [18]. The use of low refocusing flip angles further promotes phase dispersion for flowing spins [18]. It also slows the decay of the signal from stationary tissues, thereby allowing longer echo trains or a narrower echo spacing [19]. The actual scan time in MRA and 3D-TSE varies depending on the heart rate, period of minimal myocardial motion, and navigator efficiency, but was as similar as possible in each case by changing the spatial resolution in the slice encoding direction and the slice number.

2.3. Postprocessing

For all nine patients, segments 1, 2, and 3 of the RCA and 5, 6, 7, 8, 11, 13, and 15 of the LCA, as defined by American Heart Association (AHA) classification standards [26], a total of 10 coronary artery evaluation segments for each patient were assessed. Lateral branches such as segments 4, 9, 10 and 14 were not examined because these had strong variation on each case. Segments 3, 8, and 15 were classified as distal and the others were classified as proximal. Coronary vessel walls were evaluated separately in both aneurysm and normal regions and diagnosed via TTE or XCA. A coronary aneurysm was diagnosed if the internal lumen diameter was > 4.0 mm or if a distension of a part of a coronary vessel of up to one and a half times the diameter of an adjacent normal segment [6]. For each aneurysm, images from three cross-sections (center, proximal, distal portions) were obtained. As in normal regions, images of normally appearing juxta-proximal and juxta-distal points of the aneurysms and a center section of each AHA classification segment were also obtained (Fig. 2).

For evaluating the coronary vessel wall and lumen size, 3D-TSE-axi, 3D-TSE-sag, and MRA datasets were reformatted for cross-sectional images of the coronary artery on a commercial workstation (Raijin, AZE, Tokyo, Japan). To minimize digitization errors, cross-sectional images were reconstructed using 512 matrices.

2.4. Visual grading

Two board-certified radiologists with 13 and 11 years of experience independently evaluated all coronary vessel wall images. The quality of each cross-sectional coronary artery segment image was visually graded on a four-point scale as follows: 4 as excellent (no artifacts, unrestricted evaluation); 3 as good (minor artifacts, good diagnostic quality); 2 as adequate (moderate artifacts, acceptable for routine clinical diagnosis); 1 as poor (severe artifacts limiting accurate evaluation) [27]. Any discrepancies between the two readers were resolved by consensus.

2.5. Measurement of the internal diameter and wall thickness

Cross-sectional images were imported into free software (ImageJ ver. 1.50i, National Institutes of Health, USA) [28]. Two data profiles were obtained by setting the linear region of the region of interest (ROI), with one running through the short diameter and the other running through the long diameter of the coronary artery. For the baseline correction of profile data, trend removal processing was performed on the data between the minimum values outside of the vessel wall. Full width at half maximum was calculated from corrected profile data for the short and long diameters and from this the internal diameters of MRA and the internal and external diameters of 3D-TSE were calculated (Fig. 2). The final internal diameter and external diameter were then calculated as the average value of the short and long diameters. Wall thickness was calculated as follows:

$$\text{Wall thickness} = (\text{External diameter} - \text{Internal diameter})/2$$

Internal diameter and wall thickness were measured in all cases with a visual grade between 2 and 4, inclusive. The more reproducible sequence for the internal diameter of the MRA was selected from 3D-TSE-axi or 3D-TSE-sag by using the reproducibility test. A Bland-Altman plot of MRA versus 3D-TSE and a scatter plot of the internal diameter of MRA versus the wall thickness of 3D-TSE were then created for this sequence.

2.6. Measurement of contrast ratio between the lumen and wall

To evaluate the blood signal void based on the slice orientation, the

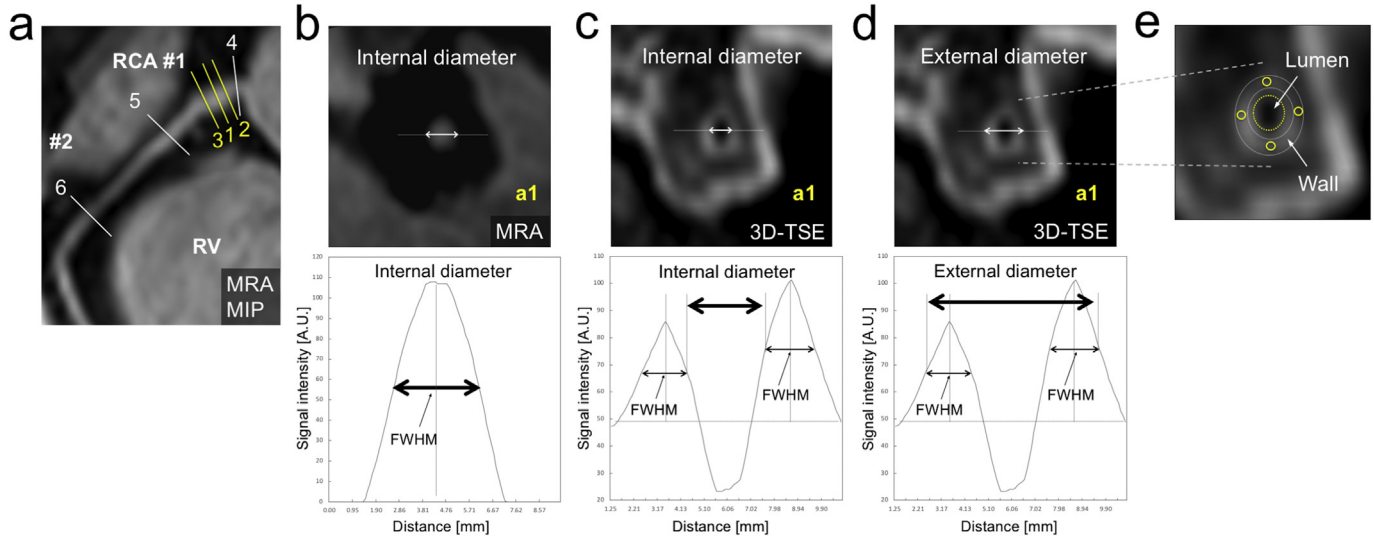

Fig. 2. The coronary magnetic resonance angiography (MRA) collapsed partial maximum intensity projection (MIP) image demonstrates the right coronary artery (RCA) segments (#) 1 and 2 in a 10-year-old girl with Kawasaki disease (KD) (a). For the measurement location, yellow and white lines indicate aneurysmal regions (1, center; 2, proximal; and 3, distal points) and normal-proximal regions (4, juxta-proximal; 5, juxta-distal; 6), respectively, defined based on the American Heart Association classification scheme. Each profile's data corresponds to a dotted line in each cross-sectional image (b, c, and d). For internal diameter measurements via MRA, full width at half maximum (FWHM) values were obtained from the profile curve (b). In 3D-TSE images, internal and external diameters were also measured using the vessel wall profile curve (c and d). Subsequently, wall thickness was measured by subtracting the internal diameter from the external diameter. In order to measure the contrast ratio between the lumen and vessel wall in 3D TSE imaging, regions of interest (ROIs) were set (e). The ROIs of the lumen and vessel wall are indicated by the yellow dotted line and solid line, respectively. (RV, right ventricle). (For interpretation of the references to colour in this figure legend, the reader is referred to the web version of this article.)

contrast ratio between the lumen and vessel wall diameters in the proximal coronary region sites was calculated; i.e., segments 1, 2, 5, 6, and 11 in 3D TSE-axi and 3D TSE-sag. As show in Fig. 2e, the circular ROI was created in the center of the lumen using 75% of the luminal area obtained from the 3D-TSE. On the vessel wall, the circular ROI was created at four points equally spaced from the circumference; the signal intensity was measured, and the average value of the four points was taken as the final value. The contrast ratio between the lumen and vessel wall was calculated as follows:

$$\text{Contrast ratio} = |\,\text{Mean}_{\text{wall}} - \text{Mean}_{\text{lumen}}\,|/|\,\text{Mean}_{\text{wall}} + \text{Mean}_{\text{lumen}}\,|,$$

where $\text{Mean}_{\text{wall}}$ and $\text{Mean}_{\text{lumen}}$ denote the mean signal intensities of the vessel and the lumen, respectively.

2.7. Statistical analyses

All statistical analyses were performed using R version 3.5.1 (The R Foundation for Statistical Computing, Vienna, Austria). To evaluate the reproducibility of internal diameters, interclass correlation coefficients (ICCs) and Bland-Altman plots were used. Fixed biases and proportional biases were defined as significant with a paired *t*-test and linear regression *P*-value of < 0.05. Correlations were used to evaluate the relationship between the internal diameter obtained from MRA and the wall thickness of 3D-TSE. The cut-off for wall thickening was 1 mm, per the field's clinical consensus [29]. A paired t-test was performed to check for differences in the contrast ratio measured for the lumen and vessel walls.

3. Results

We evaluated 164 coronary artery points in total (aneurysmal regions, 73; normal-proximal regions, 64; normal-distal regions, 27). The actual scan time for each case was approximately 8–9 min for MRA and 12–13 min for 3D-TSE-axi. 3D-TSE-sag had an increase in the number of slices as the scan time increased to approximately 13–14 min. Measurements from all patients with KD are summarized in Table 1. A total of 21 aneurysms were located in the proximal regions (4 in segment 1, 4 in segment 2, 6 in segment 5, 1 at the bifurcation of segments 5-6-11, 3 in segment 6, 1 in segment 6-7, 1 in segment 7, and 1 in segment 11). MRA had an excellent reproducibility when compared to TTE or XCA (ICC = 0.99) and as such was used for all subsequent standard internal diameter measurements.

Table 1
Patients with Kawasaki disease: TTE or XCA, and MRA measurements.

Patients (age [yr] & gender)	Aneurysms	TTE/XCA [mm]	MRA [mm]
Case 1 (10F)	Segment 1	3.8	3.7
	Segment 5	3.6	3.5
	Segment 6	3.8	3.8
	Segment 11	3.8	3.7
Case 2 (2F)	Segment 1	3.3	3.4
	Segment 5	3.6	3.8
Case 3 (9F)	Segment 2	N/A	3.2
	Segment 2	N/A	3.2
	Segment 5	4.1	4.1
Case 4 (1 M)	Segment 1	3.6	3.6
Case 5 (7 M)	Segment 1	10.6	10.1
	Segment 2	7.6	7.6
	Segment 6	6.7	6.7
Case 6 (4F)	Segment 5	4.1	5.0
	Segment 6	5.9	6.2
	Segment 7	5.6	6.5
Case 7 (2 M)	Segment 5	3.4	3.4
Case 8 (8F)	Segment 5-6-11	5.8	5.6
	Segment 6-7	7.8	7.8
Case 9 (4F)	Segment 2	3.8	3.7
	Segment 5	7.1	7.0

TTE, transthoracic echocardiography. XCA, X-ray coronary angiography. MRA, magnetic resonance angiography. N/A, not applicable.

The visual grading of 3D-TSE images is summarized in Table 2. In aneurysmal and normal-proximal regions, 3D-TSE-axi contained more grade 4 than 3D-TSE-sag. The visual grades of the distal regions were mostly grade 1 and were inappropriate for quantitative analyses, even those of the 3D-TSE-axi images (74.1%). All distal regions were thus removed from subsequent analyses.

The ICCs of the internal diameters are listed in Table 3. 3D-TSE-axi had higher ICC values than did 3D-TSE-sag for both aneurysmal and normal-proximal regions. Notably, in normal-proximal regions, 3D-TSE-sag had lower ICC values (0.32). Thus, Bland-Altman plots of the internal diameters obtained via MRA versus those obtained via 3D-TSE and scatter plots of the internal diameters obtained via MRA versus the wall thicknesses via 3D-TSE were created with 3D-TSE-axi data alone (Figs. 3 and 4). Representative 3D-TSE-axi and 3D-TSE-sag images are shown in Fig. 5.

Bland-Altman plots of the internal diameter obtained with MRA versus with 3D-TSE-axi are shown in Fig. 3. In the aneurysmal regions, the 95% limits of agreement were -0.13 to 2.89 mm. A significant fixed bias ($P < 0.001$) and proportional bias ($P = 0.002$) were found. In normal-proximal regions, the 95% limits of agreement were -0.14 to 0.57 mm. There was a significant fixed bias ($P < 0.001$) but an insignificant proportional bias ($P = 0.700$) in these regions.

Scatter plots of the internal diameters obtained via MRA versus wall thicknesses obtained via 3D-TSE-axi are shown in Fig. 4. There was a significant correlation ($r = 0.649$, $P < 0.001$) between internal diameter via MRA and wall thickness via 3D-TSE-axi in the aneurysmal regions. With a 1-mm cut-off for wall thickening, which is the cut-off most often used, 42 out of 50 (84.0%) points were found to be abnormal. No significant correlation ($r = 0.054$, $P = 0.357$) between internal diameters via MRA and wall thicknesses via 3D-TSE-axi was found in the normal-proximal regions. With a 1-mm cut-off for wall thickening, 9 out of 49 (18.4%) points were found to be abnormal.

The contrast ratios between lumen and vessel wall on 3D TSE-axi and 3D TSE-sag image are shown in Fig. 6. In segments 1, 5, 6, the 3D TSE-axi contrast ratios were significantly higher than those of 3D TSE-sag ($P = 0.015$, $P = 0.047$, and $P = 0.012$, respectively). In segment 2, 3D TSE-sag had a significantly higher contrast ratio than 3D TSE-axi ($P = 0.035$). In segment 11, 3D TSE-axi had a higher contrast ratio than 3D TSE-sag, although this difference was not significant ($P = 0.123$). Fig. 7 shows examples in which the slice orientation was related to the internal diameter and the contrast between the lumen and vessel wall.

4. Discussion

We used cardiac-triggered and real-time navigator echo methods to obtain 3D-TSE images and examine the feasibility of coronary vessel wall imaging in children with KD. We found that, using these methods, coronary walls were easily differentiated from dark-appearing blood and epicardial fat. Using internal diameter measurements from 3D-TSE images, larger aneurysmal diameters were found to lead to a larger MRA bias. This bias significantly influenced wall thickness measurements.

Suzuki et al. reported differences in the internal diameters found via XCA and 2D triple inversion-recovery (IR) TSE imaging in 12 patients with KD, though these subjects were not limited to children [8]. Using 2D dual inversion-recovery (DIR)-TSE imaging, Greil et al. revealed that vessel wall area and thickness were about two-fold greater in six children with KD than in healthy control patients [9]. These are reports of 2D imaging, and to the best of our knowledge, few studies have pursued pediatric 3D imaging. Given this background, the present study is likely the first to quantify pediatric coronary vessel wall thickness using 3D imaging.

Visualizing coronary vessel walls in children is considerably more challenging than doing so in adults. Children have small hearts and coronary arteries, higher heart rates, and increased heart motion when

Table 2
The summary of visual grading, n = 164.

	Grade	All		Aneurysm		Normal-proximal		Normal-distal	
3D-TSE-axi	4	70	(42.7%)	39	(53.4%)	28	(43.8%)	3	(11.1%)
	3	31	(19.0%)	12	(16.4%)	15	(23.4%)	4	(14.8%)
	2	7	(4.3%)	1	(1.4%)	6	(9.4%)	0	(0%)
	1	56	(34.1%)	21	(28.8%)	15	(23.4%)	20	(74.1%)
3D-TSE-sag	4	50	(30.5%)	31	(42.5%)	16	(25.0%)	3	(11.1%)
	3	38	(23.2%)	20	(27.4%)	17	(26.6%)	1	(3.7%)
	2	15	(9.1%)	6	(8.2%)	8	(12.5%)	1	(3.7%)
	1	61	(37.2%)	16	(22.0%)	23	(35.9%)	22	(81.5%)
Axi vs. sag	*P*	0.069		0.069		0.150		0.474	

3D-TSE, three-dimensional turbo spin-echo. Axi, axial. Sag, sagittal.

Table 3
The list of interclass correlation coefficients between internal diameter on MRA and 3D-TSE, n = 137.

MRA vs.	All		Aneurysm		Normal-proximal	
3D-TSE-axi	0.91	[0.78, 0.95]	0.88	[0.60, 0.95]	0.90	[0.80, 0.95]
3D-TSE-sag	0.84	[0.56, 0.92]	0.81	[0.42, 0.92]	0.32	[−0.01, 0.60]

[95% confidence interval].

compared to adults. To address and correct for heart motion, we performed retrospective cine MRI (100 phases) in the present study. We then acquired data during the mid-diastolic or systolic rest periods with cine MRI. In addition, with appropriate acquisition window parameters (e.g. a TSE factor = echo train length), coronary vessel walls were visualized in children with heart rates > 100 BPM. 3D-TSE images from any section or direction could then be reconstructed and visualized with whole-heart-imaging-derived 3D volume data. Further, when compared to 2D imaging, FOV settings were found to be more convenient and practical because they were easier to determine and required less expertise.

There have been reports on various techniques for coronary vessel wall imaging. While 2D DIR-TSE imaging is a standard method, it is not suitable for a wide range of applications and is difficult to validate or determine its reproducibility during a given examination [10–12]. On the other hand, successful applications of 3D imaging and gradient-echo (GRE) imaging using DIR or IR pulse have been reported [13–16]. 3D GRE imaging is less dependent on flow direction and velocity than is 3D-TSE imaging. However, because it is necessary to set an inversion time when using this method, two heartbeats are required to acquire an echo train length in patients with elevated heart rates. In contrast, 3D-TSE can be acquired within one heartbeat, resulting in a shorter scan time.

In terms of internal diameter and contrast measurements, 3D-TSE-axi is associated with an improved performance over 3D-TSE-sag. Flow direction and velocity are also related to the results obtained. Yoneyama et al. reported that in carotid artery vessel wall imaging using flow sensitizing to suppress the blood signal [17], suppression occurred when the flow direction was close to parallel to the slice encoding direction and did not occur when it was close to perpendicular. As shown in Fig. 6, segments 1, 5 and 6 are close to parallel by axial collection, which is consistent with the result that 3D-TSE-axi was effective in blood signal suppression. As shown in Fig. 7, if the blood signal was not suppressed using 3D-TSE-axi, it was useful to add 3D-TSE-sag.

As indicated by the Bland-Altman plots displayed here, internal diameters via 3D-TSE-axi were noticeably narrowed in aneurysmal regions. This bias was strengthened as the internal diameter grew. That

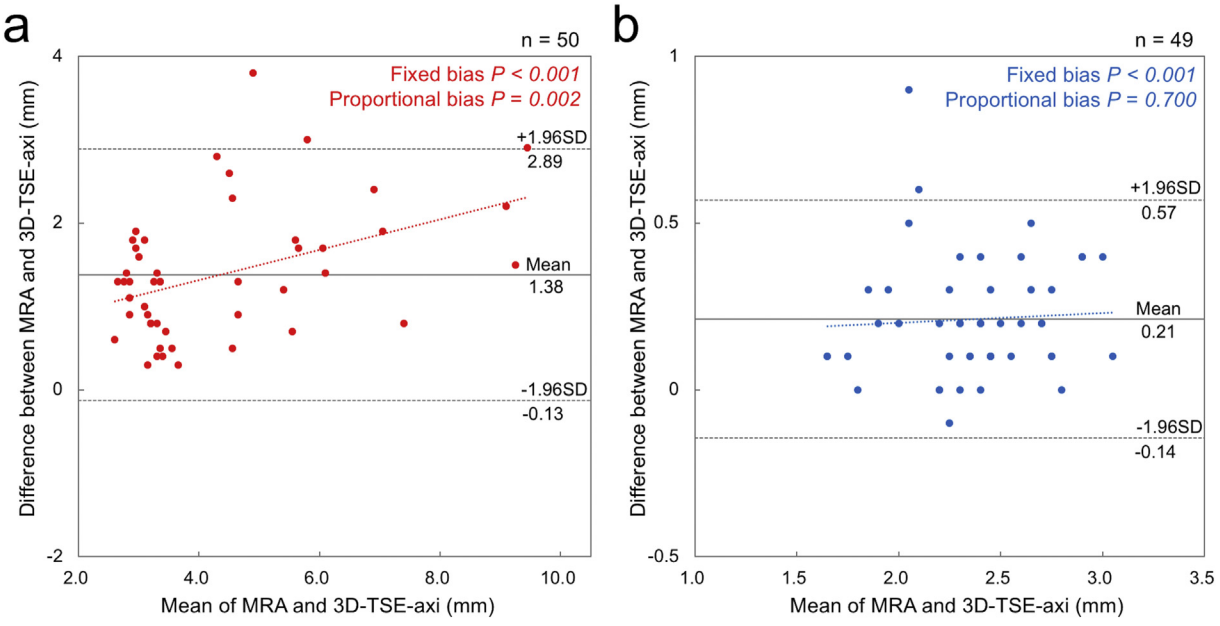

Fig. 3. Bland-Altman plots of the internal diameter determined via MRA and 3D-TSE-axi in aneurysmal (a) and normal-proximal (b) regions. Bland-Altman plots demonstrate good agreement between internal diameters via MRA and internal diameters via 3D-TSE-axi. The mean measure (MRA + 3D-TSE-axi/2) for each parameter is plotted versus the difference between MRA and 3D-TSE-axi for each case. Mean differences (solid lines) and ± 1.96 standard deviations (dotted lines) are shown.

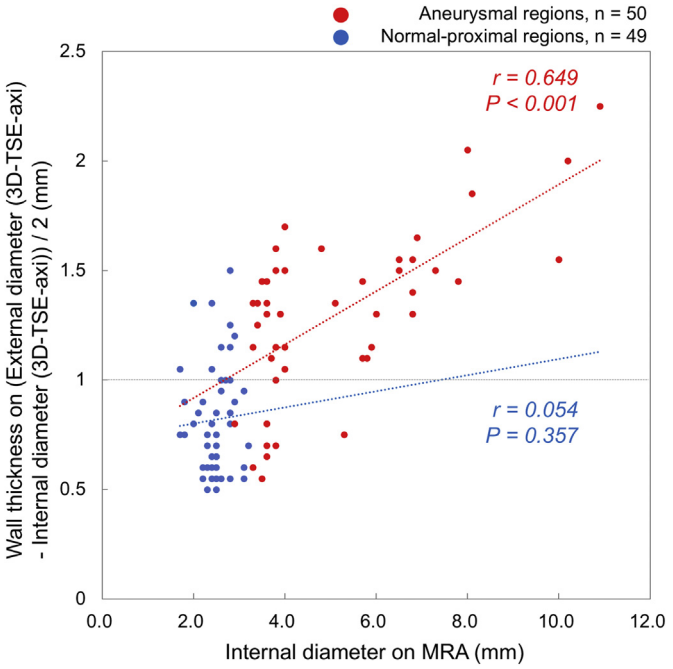

Fig. 4. Scatter plots including internal diameters per MRA and wall thickness per 3D-TSE-axi for each aneurysmal region (red dots) and each normal-proximal region (blue dots). (For interpretation of the references to colour in this figure legend, the reader is referred to the web version of this article.)

may have been due to laminar flow proximal to the vessel wall and increased turbulent flow caused by changes in the vessel lumen's shape. By contrast, in normal-proximal regions, the internal diameter via 3D-TSE-axi was found to be 0.21 mm narrower than that via MRA, though this bias was small and nonsignificant.

In wall thickness measurements, with no significant correlation found between internal diameter and wall thickness in normal-proximal regions. This supports the feasibility of coronary vessel wall imaging via 3D-TSE. By contrast, larger internal diameters in aneurysmal regions were associated with thicker wall thickness. Although this result included actual wall thickening, the frequency of wall thickening that was found using this approach (84.0%) was too high.

While this study offers significant findings of importance to the field, several limitations should also be noted. First, given that we identified no cases of thrombosed aneurysms here, the present study does not demonstrate the utility of coronary vessel wall assessments in thrombus cases. Second, we did not compare MR coronary vessel wall imaging with intravascular ultrasound [30], which is a standard approach to coronary artery wall assessments. However, intravascular ultrasound is an invasive technique with non-negligible risks, and as such is difficult to perform routinely or for experimental purposes. Finally, spatial resolution of 3D-TSE may have been insufficient in wall thickness measurements. Furthermore, our data were not isotropic. The resolution of the z-axis was lower than that of the x- and y-axes. Observations made parallel to the z-axis were good, but when the angle of separation from the z-axis increased, it may have influenced the measurements. However, it is important to note that there is a trade-off between higher-resolution imaging and an increased scan time, which can increase patient discomfort.

5. Conclusions

We report here that coronary vessel wall imaging by 3D-TSE using cardiac-triggered and real-time navigator echo methods results in the expected range being obtained in normal-proximal regions of the coronary artery in children and that this method also offers versatile axial slice orientations. However, in aneurysmal regions, larger aneurysmal diameters led to a greater discrepancy between MRA and 3D-TSE findings. In 3D-TSE, wherein blood flow suppression may be insufficient, careful wall thickness assessments should be performed, especially in large aneurysm cases. The method proposed here may be used as an approach for the evaluation of coronary vessel walls in KD, which have proven difficult to visualize thus far. Taken together, these

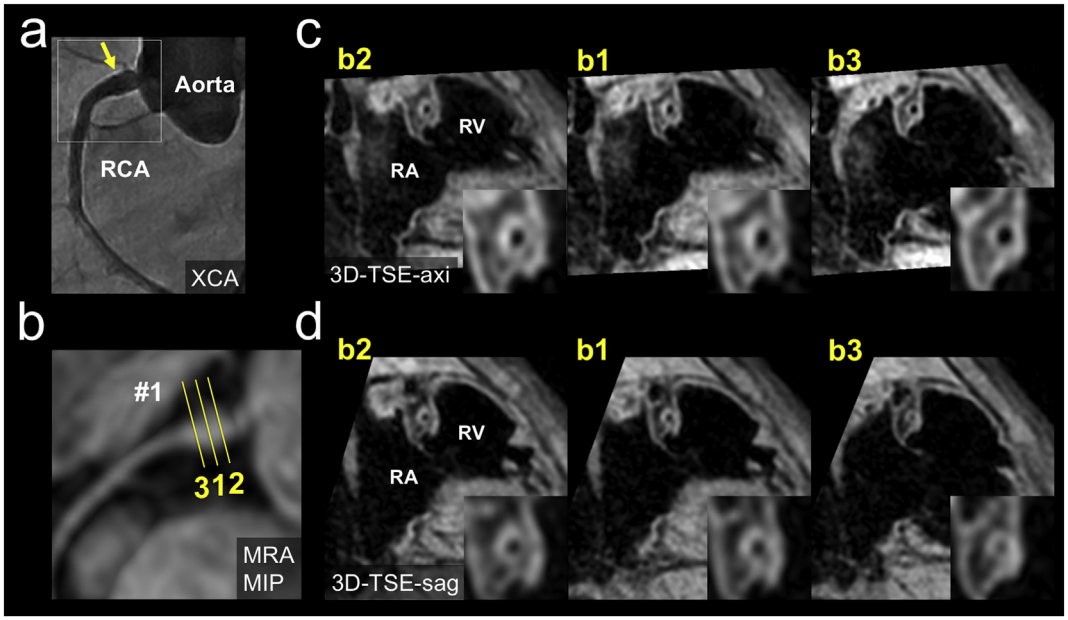

Fig. 5. The X-ray coronary angiography (XCA) images demonstrate coronary artery aneurysm (arrow, RCA#1, 3.3 mm) in a 30-month-old girl with KD (a). In the MRA collapsed partial MIP image, yellow lines indicate aneurysmal regions (b). Each cross-sectional image in 3D-TSE-axi and 3D-TSE-sag correspond to the solid line numbers in the MRA images (c and d). In the center of the aneurysm, the internal diameter on MRA was 3.4 mm, which was close to that of XCA. The internal diameter on 3D-TSE-axi was 2.7 mm, which was narrower than that of XCA and MRA. The internal diameter on 3D-TSE-sag was 2.6 mm, which was narrower than that of 3D-TSE-axi. (RA, right atrium; RV, right ventricle). (For interpretation of the references to colour in this figure legend, the reader is referred to the web version of this article.)

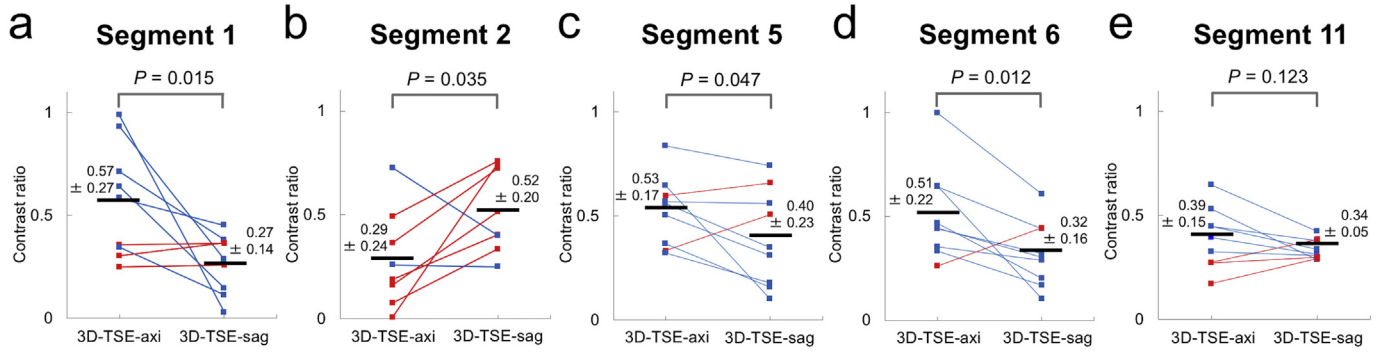

Fig. 6. Measurement of the contrast ratio between the lumen and vessel wall of segments 1, 2, 5, 6, and 11 on 3D TSE-axi and 3D TSE-sag in nine children with KD. In segment 2, since the scan range was lost in one patient, it was measured in 8 patients. When 3D TSE-axi has a higher contrast ratio than 3D TSE-sag, it is indicated by a blue line. When 3D TSE-sag has a higher contrast ratio than 3D TSE-axi, it is indicated by a red line. (For interpretation of the references to colour in this figure legend, the reader is referred to the web version of this article.)

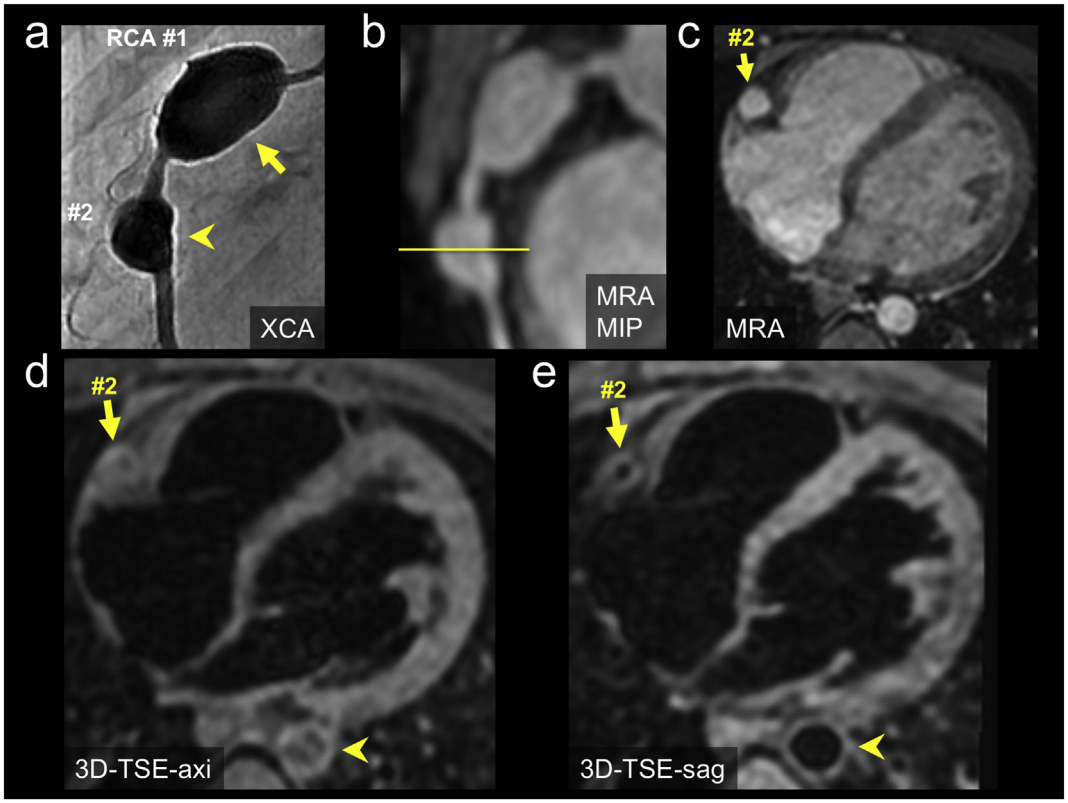

Fig. 7. The XCA (a) and the MRA collapsed partial MIP image (b) of RCA demonstrates two aneurysms (proximal, 10.6 mm; distal, 7.6 mm) of segment 1 and 2 in a 7-year-old boy with KD (arrow and arrowhead, a). The original MRA image (C), 3D TSE-axi (d), and MPR image of 3D TSE-sag (e) were axial images at the same position (yellow line on MRA). In these axial images, a cross-sectional view of the aneurysm of segment 2 is clearly depicted (arrow, c-e). In the original 3D TSE-axi image, the lumen of an aneurysm and descending aorta are not clear (arrow and arrowhead, d). In contrast, in the 3D TSE-sag MPR image, the lumen of an aneurysm and descending aorta are clearly depicted (arrow and arrowhead, e). (For interpretation of the references to colour in this figure legend, the reader is referred to the web version of this article.)

results may have implications with regard to the speed and quality of pediatric care in KD.

Declaration of Competing Interest

We have no potential conflict of interest.

Acknowledgements

The authors would like to thank the staff of the Department of Radiology at Chiba University Hospital for helping with the MR imaging data acquisition. The authors would like to thank, Clinical Application Marketer, Atsushi Takemura at Philips Corporation for providing information about 3D-TSE imaging. Finally, the authors would like to thank the anonymous reviewers for their valuable comments.

Ethical approval

This study was approved by our local ethics review board.

References

[1] Newburger JW, Takahashi M, Gerber MA, Gewitz MH, Tani LY, Burns JC, et al.

Diagnosis, treatment, and long-term management of Kawasaki disease: a statement for health professionals from the Committee on Rheumatic Fever, Endocarditis, and Kawasaki Disease, Council on Cardiovascular Disease in the Young, American Heart Association. Pediatrics 2004;114:1708–33.
[2] Akagi T, Ogawa S, Ino T, Iwasa M, Echigo S, Kishida K, et al. Catheter interventional treatment in Kawasaki disease: a report from the Japanese Pediatric Interventional Cardiology Investigation group. J Pediatr 2000;137:181–6.
[3] Kitamura S. The role of coronary bypass operation on children with Kawasaki disease. Coron Artery Dis 2002;13:437–47.
[4] Kato H, Ichinose E, Yoshioka F, Takechi T, Matsunaga S, Suzuki K, et al. Fate of coronary aneurysms in Kawasaki disease: serial coronary angiography and long-term follow-up study. Am J Cardiol 1982;49:1758–66.
[5] Takemura A, Suzuki A, Inaba R, Sonobe T, Tsuchiya K, Omuro M, et al. Utility of coronary MR angiography in children with Kawasaki disease. AJR Am J Roentgenol 2007;188:W534–9.
[6] Mavrogeni S, Papadopoulos G, Douskou M, Kaklis S, Seimenis I, Baras P, et al. Magnetic resonance angiography is equivalent to X-ray coronary angiography for the evaluation of coronary arteries in Kawasaki disease. J Am Coll Cardiol 2004;43:649–52.
[7] Greil GF, Stuber M, Botnar RM, Kissinger KV, Geva T, Newburger JW, et al. Coronary magnetic resonance angiography in adolescents and young adults with Kawasaki disease. Circulation 2002;105:908–11.
[8] Suzuki A, Takemura A, Inaba R, Sonobe T, Tsuchiya K, Korenaga T. Magnetic resonance coronary angiography to evaluate coronary arterial lesions in patients with Kawasaki disease. Cardiol Young 2006;16:563–71.
[9] Greil GF, Seeger A, Miller S, Claussen CD, Hofbeck M, Botnar RM, et al. Coronary magnetic resonance angiography and vessel wall imaging in children with Kawasaki disease. Pediatr Radiol 2007;37:666–73.
[10] Fayad ZA, Fuster V, Fallon JT, Jayasundera T, Worthley SG, Helft G, et al. Noninvasive in vivo human coronary artery lumen and wall imaging using black-blood magnetic resonance imaging. Circulation 2000;102:506–10.
[11] Botnar RM, Stuber M, Kissinger KV, Kim WY, Spuentrup E, Manning WJ. Noninvasive coronary vessel wall and plaque imaging with magnetic resonance imaging. Circulation 2000;102:2582–7.
[12] Miao C, Chen S, Macedo R, Lai S, Liu K, Li D, et al. Positive remodeling of the coronary arteries detected by magnetic resonance imaging in an asymptomatic population: MESA (Multi-Ethnic Study of Atherosclerosis). J Am Coll Cardiol 2009;53:1708–15.
[13] Kim WY, Stuber M, Börnert P, Kissinger KV, Manning WJ, Botnar RM. Three-dimensional black-blood cardiac magnetic resonance coronary vessel wall imaging detects positive arterial remodeling in patients with nonsignificant coronary artery disease. Circulation 2002;106:296–9.
[14] Botnar RM, Kim WY, Börnert P, Stuber M, Spuentrup E, Manning WJ. 3D coronary vessel wall imaging utilizing a local inversion technique with spiral image acquisition. Magn Reson Med 2001;46:848–54.
[15] Ishimoto T, Taniguchi Y, Miyati T, Kawakami M, Ishihara M. Non-contrast coronary artery wall and plaque imaging using inversion-recovery prepared steady-state free precession. BMC Med Imaging 2015;15:26.
[16] Katoh M, Spuentrup E, Buecker A, Schaeffter T, Stuber M, Günther RW, et al. MRI of coronary vessel walls using radial k-space sampling and steady-state free precession imaging. AJR Am J Roentgenol 2006;186:S401–6.
[17] Yoneyama M, Nakamura M, Tabuchi T, Takemura A, Obara M. Optimization of 3D-variable refocusing flip angle RARE imaging for high-resolution volumetric black-blood angiography. Radiol Phys Technol 2012;5:270–6.
[18] Storey P, Atanasova IP, Lim RP, Xu J, Kim D, Chen Q, et al. Tailoring the flow sensitivity of fast spin-echo sequences for noncontrast peripheral MR angiography. Magn Reson Med 2010;64:1098–108.
[19] Busse RF, Brau AC, Vu A, Michelich CR, Bayram E, Kijowski R, et al. Effects of refocusing flip angle modulation and view ordering in 3D fast spin echo. Magn Reson Med 2008;60:640–9.
[20] Fan Z, Zhang Z, Chung YC, Weale P, Zuehlsdorff S, Carr J, et al. Carotid arterial wall MRI at 3T using 3D variable-flip-angle turbo spin-echo (TSE) with flow-sensitive dephasing (FSD). J Magn Reson Imaging 2010;31:645–54.
[21] Qiao Y, Steinman DA, Qin Q, Etesami M, Schär M, Astor BC, et al. Intracranial arterial wall imaging using three-dimensional high isotropic resolution black blood MRI at 3.0 Tesla. J Magn Reson Imaging 2011;34:22–30.
[22] Mihai G, Chung YC, Merchant A, Simonetti OP, Rajagopalan S. T1-weighted-SPACE dark blood whole body magnetic resonance angiography (DB-WBMRA): initial experience. J Magn Reson Imaging 2010;31:502–9.
[23] Stuber M, Botnar RM, Danias PG, Kissinger KV, Manning WJ. Submillimeter three-dimensional coronary MR angiography with real-time navigator correction: comparison of navigator locations. Radiology 1999;212:579–87.
[24] Capannari TE, Daniels SR, Meyer RA, Schwartz DC, Kaplan S. Sensitivity, specificity and predictive value of two-dimensional echocardiography in detecting coronary artery aneurysms in patients with Kawasaki disease. J Am Coll Cardiol 1986;7:355–60.
[25] Hinks RS, Constable RT. Gradient moment nulling in fast spin echo. Magn Reson Med 1994;32:698–706.
[26] American Heart Association. Report of the Ad Hoc Committee for Grading of Coronary Artery Disease: a reporting system on patients evaluated for coronary artery disease. Circulation 1975;5:5–40.
[27] Kim JW, Goo HW. Coronary artery abnormalities in Kawasaki disease: comparison between CT and MR coronary angiography. Acta Radiol 2013;54:156–63.
[28] Abràmoff MD, Magalhães PJ, Ram SJ. Image processing with ImageJ. Biophotonics Int 2004;11:36–42.
[29] Gradus-Pizlo I, Bigelow B, Mahomed Y, Sawada SG, Rieger K, Feigenbaum H. Left anterior descending coronary artery wall thickness measured by high-frequency transthoracic and epicardial echocardiography includes adventitia. Am J Cardiol 2003;91:27–32.
[30] Suzuki A, Yamagishi M, Kimura K, Sugiyama H, Arakaki Y, Kamiya T, et al. Functional behavior and morphology of the coronary artery wall in patients with Kawasaki disease assessed by intravascular ultrasound. J Am Coll Cardiol 1996;27:291–6.